

Article

Characteristics of Doped TiO₂ Nanoparticle Photocatalysts Prepared by the Rotten Egg White

Chung-Ming Lu ^{1,2}, Raju Kumar Sharma ^{2,3} , Pin-Yun Lin ³, Yi-Hsun Huang ² , Jung-Sheng Chen ⁴ ,
Wen-Chien Lee ^{1,*} and Chien-Yen Chen ^{2,5,*} 

¹ Department of Chemical Engineering, National Chung Cheng University, 168 University Road, Min-Hsiung, Chiayi 62102, Taiwan; n0935718023@gmail.com

² Department of Earth and Environmental Sciences, National Chung Cheng University, 168 University Road, Min-Hsiung, Chiayi 62102, Taiwan; raju28212@gmail.com (R.K.S.); x699237014x@gmail.com (Y.-H.H.)

³ Department of Chemistry and Biochemistry, National Chung Cheng University, 168 University Road, Min-Hsiung, Chiayi 62102, Taiwan; kittycat1604@hotmail.com

⁴ Department of Medical Research, E-Da Hospital, Kaohsiung 82445, Taiwan; ed113187@edah.org.tw

⁵ Center for Innovative Research on Aging Society, AIM-HI, National Chung Cheng University, 168, University Rd., Min-Hsiung, Chiayi 62102, Taiwan

* Correspondence: chmwcl@ccu.edu.tw (W.-C.L.); chien-yen.chen@oriel.oxon.org or yen@eq.ccu.edu.tw (C.-Y.C.); Tel.: +886-5-2720411 (ext. 66220) (C.-Y.C.); Fax: +886-5-2720807 (C.-Y.C.)

Abstract: In this study, expired egg white was used as a template, and a sol–gel method was employed to prepare pure-phase TiO₂ nano-powder and mixed-phase powders doped with NaF and NaI. The influences of different calcination temperatures, doping elements, and doping amounts during the preparation process on the photocatalytic performance and activity of the prepared TiO₂ powders were studied. The results of the experiments showed that the F-doped TiO₂ had the highest photocatalytic activity when the doping amount was 1.2%, as examined by EDS, where the sintering temperature was 500 °C. F-doped TiO₂ nanoparticles were also synthesized by the sol–gel method using tetrabutyl titanate and NaF mixed with expired egg white protein as the precursor. The F-TiO₂ photocatalyst was characterized using FE-SEM, HR-TEM, EDS, XPS, and UV-Vis, and the photocatalytic activity was evaluated by photodegradation of methylene blue under visible light. The results showed that doping with F reduced the energy band gap (3.04 eV) of TiO₂, thereby increasing the photocatalytic activity in the visible-light region. The visible-light wavelength range and photocatalytic activity of the catalyst were also affected by the doping amount.

Keywords: TiO₂ nano-powders; F-doped TiO₂ nanoparticles; sol–gel method; photocatalyst



Citation: Lu, C.-M.; Sharma, R.K.; Lin, P.-Y.; Huang, Y.-H.; Chen, J.-S.; Lee, W.-C.; Chen, C.-Y.

Characteristics of Doped TiO₂ Nanoparticle Photocatalysts Prepared by the Rotten Egg White. *Materials* **2022**, *15*, 4231. <https://doi.org/10.3390/ma15124231>

Academic Editors: Jose L. Hueso and Ewa Kowalska

Received: 12 May 2022

Accepted: 9 June 2022

Published: 15 June 2022

Publisher's Note: MDPI stays neutral with regard to jurisdictional claims in published maps and institutional affiliations.



Copyright: © 2022 by the authors. Licensee MDPI, Basel, Switzerland. This article is an open access article distributed under the terms and conditions of the Creative Commons Attribution (CC BY) license (<https://creativecommons.org/licenses/by/4.0/>).

1. Introduction

In 1972, Fujishima and Honda discovered that irradiated TiO₂ particles can cause continuous oxidation–reduction reactions in water. Taking this as an opportunity, a new era of heterogeneous catalysis research began. Since the 1990s, great progress has been made in TiO₂ photocatalysis research in terms of the photocatalytic removal of water- and gas-phase organic and inorganic pollutants in the field of environmental protection, and this is considered to be a promising technology for deep purification of environmental pollution. In particular, the recent COVID-19 virus is raging, and there have been related studies using TiO₂ photocatalysis that have made research contributions in the field of health and hygiene [1].

Due to the wide band gap of TiO₂, the catalytic activity is generally not high under sunlight. The material needs to be scientifically modified so that the material can produce catalysis in the range of visible light. For this reason, many researchers have assessed various scientific methods for the preparation and modification of TiO₂ photocatalysts, using different preparation methods or preparation conditions, in addition to related

technologies such as doping of different elements, semiconductor compounding, and the introduction of template agents. Through this research, the photocatalytic activity of TiO_2 may be able to be improved, and semiconductor-based research on photocatalysis has received extensive attention [2–7]. Element-doped TiO_2 is regarded as a promising way in which to obtain a more effective photocatalyst. In this study, F-doped TiO_2 was synthesized by the sol–gel method, demonstrating both a high adsorption capacity and high photocatalytic activity under simulated sunlight irradiation. Most prior studies have been carried out under ultraviolet (UV) light, because TiO_2 photocatalysts show a relatively high activity and chemical stability under UV light, exceeding the band gap energy in the rutile or anatase phase of 3.0 or 3.2 eV, respectively. As this part of UV light (300–400 nm) only accounts for 4–6% of solar energy, the utilization rate of solar energy is quite low. Considering practical application, the visible light activity of TiO_2 must be improved. For this reason, related research has used metal or non-metal doping to modify the properties of TiO_2 in order to improve the visible light utilization of TiO_2 . Since Asahi, et al. [8] reported that non-metallic N-doped TiO_2 achieved visible light activity, research into non-metal doping has been very active [9–11], in particular, the use of expired eggs as a template [12] in doped TiO_2 research has also been reported.

Sol–gel method refers to the precursor substances such as water-soluble salt or oil-soluble alkoxide dissolved in water or organic solvent to form a homogeneous solution. Interestingly, the nanomaterials can be prepared as smaller and more uniform particles at room temperature, which meets the conditions of simple industrial manufacturing and lower cost. Due to the low temperature of this preparation method, large doses of inorganic and organic substances are allowed to be doped [13–16]. However, a new type of element-doped TiO_2 photocatalyst was prepared using sol–gel method, and this study also analyzed the mechanism of TiO_2 photocatalysis, examined related preparation methods, and investigated methods by which to improve its photocatalytic activity, such as doping and compounding, with the aim of further expanding the application of TiO_2 photocatalysis in the future. The sol–gel preparation method used in this work is popular because it is simple, less time-consuming than other methods, and operates under normal atmospheric temperature, and the process of synthesizing nanomaterials is easy and convenient [6,17,18]. The new F-doped TiO_2 photocatalytic catalyst prepared in this work was tested under UV-visible irradiation and in MB photo reactivity experiments, and it was found to have a good reaction effect in the visible light range. At the same time, we used various analytical instruments, including FE-SEM, HR-TEM, XPS, and EDS, and compared the doped TiO_2 photocatalyst with commercial-grade P-25 TiO_2 powder to verify the relationship between its chemical properties and physical properties. In addition, looking at recent research reports, F-doped TiO_2 material has a high “energy-saving” value. In order to reduce the energy consumption required for cooling in the hot summer, it would be of great value to find a new type of building near-infrared shielding material. F-doped TiO_2 nanocrystals represent a new type of energy-saving window coating with an enhanced near-infrared (NIR) shielding performance [19]. In addition, F-doped TiO_2 also has a high “environmental protection” value. The degradation of toxic dyes by F-doped TiO_2 can be improved by photochemical activity [20].

With an eye to attaining the objective of a green approach in nanobiotechnology, an expired egg white protein (EWP) biological template was used as the raw material from which to derive the precursor solution for synthesis of the photocatalyst nanoparticle material. A simple sol–gel process was used in a bottom-up approach, which involved testing different solution pH values, solution concentrations, drying times, and calcination temperatures for the synthesis of TiO_2 nanomaterials. The physicochemical properties of the various photocatalyst TiO_2 synthetic particles obtained were studied, such as the crystal structure, doping of different substances, absorption rates in the UV and visible light ranges, and under simulated sunlight ranges and their morphology, such as the shape and size of the catalyst particles, etc.

2. Materials and Methods

2.1. Chemicals and Reagents

Chemical reagents NaF (sodium fluoride, 99% purity; Acros, Geel, Belgium) and NaI (sodium iodide, 99% purity; Alfa Aesar, Ward Hill, MA, USA) were used to prepare the doping substances for use with the precursor solution. 25 wt.% of AA, ethyl alcohol (99.5%; Assay, Tainan city, Taiwan) and titanium (IV) n-butoxide, 99.0% purity; Acros) were used for material synthesis. Methylene blue (96.0% purity; Fluka, Dresden, Germany) was used to prepare a 10ppm blue aqueous solution for photocatalytic reaction testing. All chemical reagents were used without further purification.

2.2. Preparation of TiO₂ Nanoparticles Using Egg White Protein

Using titanium (IV) n-butoxide as the main raw material, absolute ethanol as the dispersion medium, and acetic acid as the inhibitor, gels of titanium dioxide and doped TiO₂ were prepared under different reaction conditions. The absolute ethanol and butyl titanate were mixed thoroughly and uniformly to prepare solution A. To prepare solution B, absolute ethanol, acetic acid, and expired egg white (or deionized water) were mixed evenly. Then, under vigorous stirring, solution A was added to solution B slowly in a dropwise manner and stirred for 30 min more. After the addition was completed, stirring was further continued approximately 5 min to form the gel, followed by aging for several hours at room temperature to obtain a wet gel of titanium dioxide. This wet gel was then placed in a drying box for several hours to remove the water, organic solvents, and reaction by-products in the gel to obtain TiO₂ as a dry gel. The dry gel of TiO₂ was fully grounded and calcinated at 500 °C using muffle furnace. In the heating process, the dry gel product first removes the water and alcohol adsorbed on the surface at low temperature, and then oxidizes the alkoxy groups at 280~300 °C. Furthermore, at a temperature above 400~500 °C (after more than 5 h), the hydroxyl group in the sample structure is removed. Via the calcination process, an active TiO₂ catalyst was formed [21].

2.3. Doping of NaF and NaI in TiO₂ Powder

Solution A and solution B were prepared separately, as described above. In case of NaF and NaI doping, the prepared solution B was doped with 0.5 g of NaF/NaI in 20 mL of double deionized water. To be continued, the prepared solution was uniformly mixed with above prepared solution A at the same time, using ultrasonication to form the dry gel. The formation of dry gel was dried to remove the water and it becomes a dry solid block. It should be noted that the drying time required after the sol state has formed varies according to the type of doped TiO₂ catalyst to be prepared. For example, when using EWP as the template for the F-doped TiO₂ catalyst, a longer drying time is required, because when acetylacetone is added, the proper precursor is obtained by controlling the rate of the hydrolysis reaction of Ti(OBu)₄, and the drying time required for this production process is 2~3 days. We carefully mashed the solid block material with an agate mortar, grinding it into as fine a powder as possible, and calcinated at 500 °C. In the process of heating, drying, and calcining the samples containing doping-compound and EWP, the dried gel material first removes the water and alcohol adsorbed on the surface at a low temperature, and then oxidation of the alkoxy group occurs at about 300 °C, and then at a higher temperature of about 500 °C (after 5 h or more), the hydroxyl group in the structure is removed. Therefore, in the process of calcination, an active doped TiO₂ catalyst is formed, such as the successful F-doping of TiO₂.

2.4. Photocatalytic Degradation of Methylene Blue on Photoirradiation of TiO₂ Powder

In order to confirm the degradation ability of the prepared TiO₂ photocatalyst, a dye photocatalytic degradation experiment was carried out. First, a total of 500 mL of 10 mg/L methylene blue solution was prepared and placed in five 50 mL light bottles. Then, 40 mL of MB were added to each of the five bottles, which contained 40 mg of catalyst, and the

bottles were subjected to magnetic stirring. After standing for 10/30 min in a dark room, the photocatalytic status of the samples was examined when not illuminated.

The photocatalysis test was then performed again, using a light source consisting of a kind of simulated sunlight through a filter. The reaction time under the laboratory-simulated visible light was observed after ten minutes, where 1 mL of samples were taken every ten minutes, and each removed sample was subjected to high-speed centrifugation at a rotating speed $5000 \times g$ rpm for 5 min to obtain the supernatant, and a UV-Visible spectrophotometer with a wavelength of 665 nm was employed for analysis of each supernatant samples.

2.5. Characterization

2.5.1. Analysis of Crystallization, Particle Size, Appearance, and Surface Dispersion of the Synthesized Catalyst by Scanning Electron Microscopy (SEM)

The doping component within the TiO_2 structure, particle shape, and surface distribution of the synthesized materials was observed and determined by SEM following the procedure of Bayan et al. [22]. The surface morphology of the TiO_2 photocatalyst was evaluated using a field emission scanning electron microscope (FE-SEM; Hitachi S4800-I instrument, Tokyo, Japan) with a coating of precious metal Pt at the operating range of 0.1–30 kV [23].

2.5.2. Estimation of Morphology of Synthesized Material by HR-TEM-EDX

Transmission electron microscopy (TEM) was used to observe the particle size of the catalyst and the distribution of the doped substances, and selected area electron diffraction (SAED) was employed to analyze whether the material was polycrystalline, single-crystal, or two-crystal mixed-phase. The instrument was equipped with an X-ray energy dispersive spectrometer (EDS), which was employed for elemental qualitative and quantitative analysis. Morphological study of the synthesized TiO_2 photocatalyst was conducted using a high-resolution transmission electron microscope (HR-TEM) (JEOL JEM-2010, Chiayi, Taiwan) with an acceleration voltage of 200 kV [24].

2.5.3. Estimation of Elemental Quantification of Synthesized Material by XPS

The chemical state of the atoms on the surface of the photocatalyst and elemental quantification of the synthesized material were estimated by high-resolution X-ray photoelectron spectroscopy (XPS; PHI Hybrid Quantera, Chanhassen, MN, USA), which analyzes the elements and chemical bonds on the surface of a material and is used to perform elemental quantification. Al $K\alpha$ radiation was used in XPS as a monochromatic X-ray beam of light with 49.3 W, 45.0° , and 280.00 eV.

2.5.4. Estimation of Synthesized Material Absorption by UV-VIS-NIR

UV/visible spectrometry (UV-VIS-NIR) analyzes the absorbance of light, and the results were helpful to inform the selection of the light source in this study. This instrument uses BaSO_4 as the background value to zero, and the catalyst powder is then placed in the middle of the instrument. When UV and visible light irradiate the surface of the catalyst separately, electrons in different molecules absorb different energies and produce refraction, reducing the refractive index and wavelength. The results were drawn into a graph, and the refractive index graph was converted into a yield graph through the Kubelka–Munk formula. The absorption of TiO_2 and the doped TiO_2 synthesized material was estimated using UV-VIS-NIR. A UV-VIS-NIR spectrometer (HITACHI U4100, Japan) was used to record (wavelength range = 200–2600 nm) the reflectance spectra of the samples, with BaSO_4 as a reference sample and with constant temperature through cooling Pbs Gain detector.

2.5.5. Photocatalytic Activity Measurements

A photocatalytic reactor was equipped with a simulated sunlight lamp, and the photocatalytic activity of the catalyst was characterized by the degradation rate of methylene

blue solution under irradiation by the 60 W lamp. Experiments were carried out at room temperature in quartz glass beakers. Forty ml of MB aqueous solution was added to glass bottles containing 40 mg of TiO₂ catalyst, and the bottles were subjected to magnetic stirring. After irradiation for a period of time under a simulated sun lamp at a distance of 10 cm, the samples were centrifuged, and the supernatants were removed. The absorbance was measured using a PRO739, TU-1900 dual-beam UV-visible spectrophotometer. Using the absorbance and concentration curves of methylene blue, the concentration of the methylene blue solution after degradation was obtained.

3. Results and Discussion

3.1. Morphologic Analysis of Material by SEM

3.1.1. Effects of 400 °C and 500 °C Calcination

Figure 1 below presents SEM images of TiO₂ photocatalysts prepared at different calcination temperatures (400 °C and 500 °C). It can be seen from the figure that the TiO₂ prepared at the higher calcination temperature presented a relatively uniform granular morphology and had a good dispersibility and a small agglomerate size of only 40–100 nm. The TiO₂ prepared by calcination at the lower temperature had a poor dispersibility, and there was more obvious agglomeration, with an agglomerate size of 100–300 nm. Therefore, according to the experimental results, when comparing the material after calcination at 400 °C and 500 °C, as the calcination temperature increased, the degree of agglomeration of TiO₂ decreased.

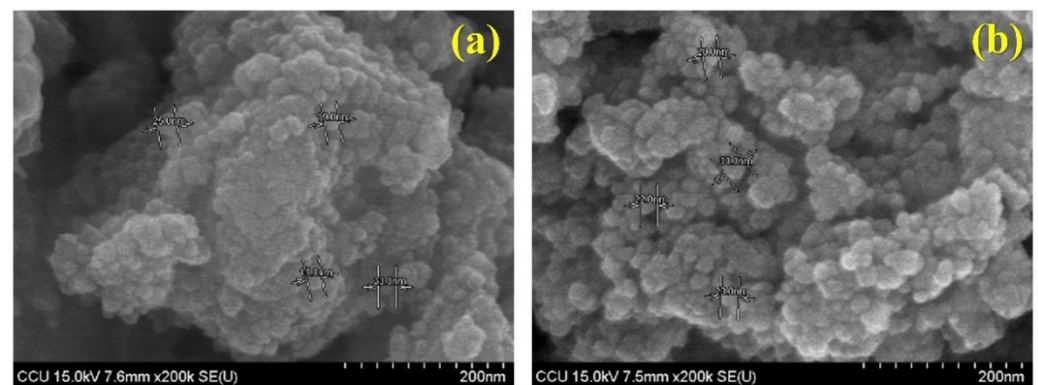


Figure 1. Field emission-scanning electron micrographs of bio-templated TiO₂ nanoparticles: (a) 400 °C and (b) 500 °C.

3.1.2. Analysis of TiO₂ and F-Doped TiO₂ by SEM

Figure 2 below presents SEM images of the TiO₂ and F-doped TiO₂ photocatalysts. It can be seen from the figure that the TiO₂ modified by F-doping had a uniform granular morphology, with good dispersibility and a small agglomerate size. After calcination at 500 °C, the agglomerates were observed to be only 10–30 nm in size. However, the unmodified TiO₂ had a poor dispersibility, and there was more obvious agglomeration after calcination at 500 °C, the size of the agglomerates being 30–50 nm. More notably, the F-doped TiO₂ crystal shape created in our laboratory is not mentioned in the current literature, and this can therefore be said to be a pioneering work. The shape obtained was particularly strange; however, photo-reactivity testing using MB strongly proved the effects to be the same. According to the results of the experiment, as the calcination temperature increased (comparing 400 °C and 500 °C), the degree of agglomeration of TiO₂ decreased. The F-doped TiO₂ particles prepared by firing at 500 °C were still uniform; the degree of agglomeration between the particles was low, and the nanoparticles were relatively uniform. However, agglomeration of undoped TiO₂ prepared under the same conditions was aggravated, indicating that F-doping can effectively inhibit the agglomeration of TiO₂ particles. In addition, after calcination at 500 °C, the F-doped TiO₂ had smaller

nanoparticles and exhibited good dispersibility. A better dispersibility can promote the activity of the photocatalyst.

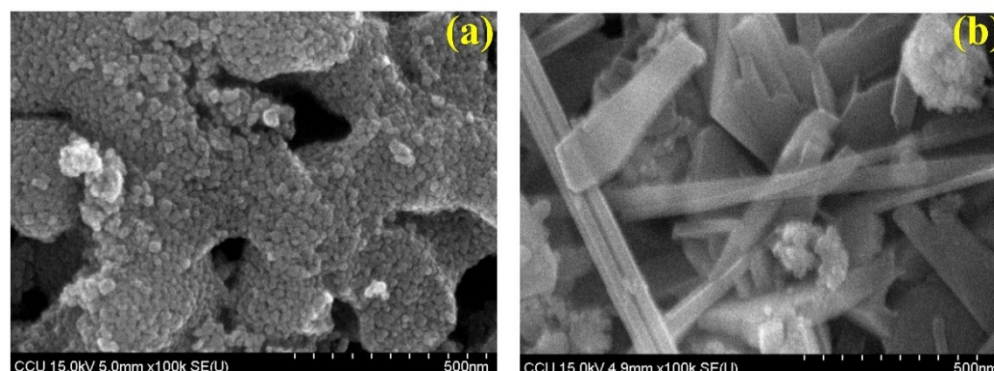


Figure 2. Field emission-scanning electron micrographs of bio-templated photocatalyst at 500 °C: (a) TiO₂ and (b) F-doped TiO₂.

3.2. Material Morphology and Elemental Signature

3.2.1. F-Doped TiO₂

The surface morphologies of TiO₂ prepared at different calcination temperatures and TiO₂ modified by doping with F are clearly shown on the SEM micrographs. In this experiment, a higher calcination temperature of 500 °C was used in order to reduce agglomeration and prepare more uniform and smaller photocatalyst nanoparticles. In addition to using SEM to understand the sample surface and its composition, in order to further study the morphology of the nanoparticles, a stronger electron beam was projected onto the TiO₂ sample. Transmission electron microscopy (TEM) provides information about the internal structure of a sample, such as crystal structure, morphology, and stress state.

In addition to the special bamboo-like shape of the F-doped TiO₂ prepared using EWP as the template, the nanoparticles were also very small, only 10–20 nm, and sometimes in the single digits at less than 10 nm. Compared with materials synthesized in other works, such as N, F-doped TiO₂ nanomaterials at around 20 nm [25], and Zn-F-doped TiO₂ [22,26], the F-doped TiO₂ prepared using expired eggs in this experiment had a special bamboo-like shaped appearance and an unusual structure, and in particular the particles were also the smallest of those synthesized previously.

The following Figure 3 shows TEM images for analysis and comparison: (a) using EWP as the template and (b) F-doped TiO₂ nanoparticle structure morphology. TEM enabled visualization of the (a) undoped and (b) F-doped samples. It is obvious that there were large differences between the undoped and F-doped particles, whatever the preparation method. The size of the F-doped TiO₂ nanoparticles was only 10–15 nm, smaller than the undoped TiO₂ particles (about 20–30 nm on average).

3.2.2. I-Doped TiO₂

In this study, in addition to using EWP as the template and NaF as an additive chemical for doping, NaI was also applied as a chemical agent to prepare I-doped TiO₂. Analysis of the I-doped TiO₂ showed in the UV-VIS-NIR test that there was no obvious absorption in the visible light region. However, the TiO₂ nanoparticles prepared by doping with I were also relatively small in Figure 4. According to analysis of the results of TEM, the average size of this type of photocatalyst nanoparticle was 15–20 nm. It can be speculated that the smaller the catalyst particle, relatively, the larger the specific surface area, and this will play a greater role in the reaction efficiency of the photocatalyst.

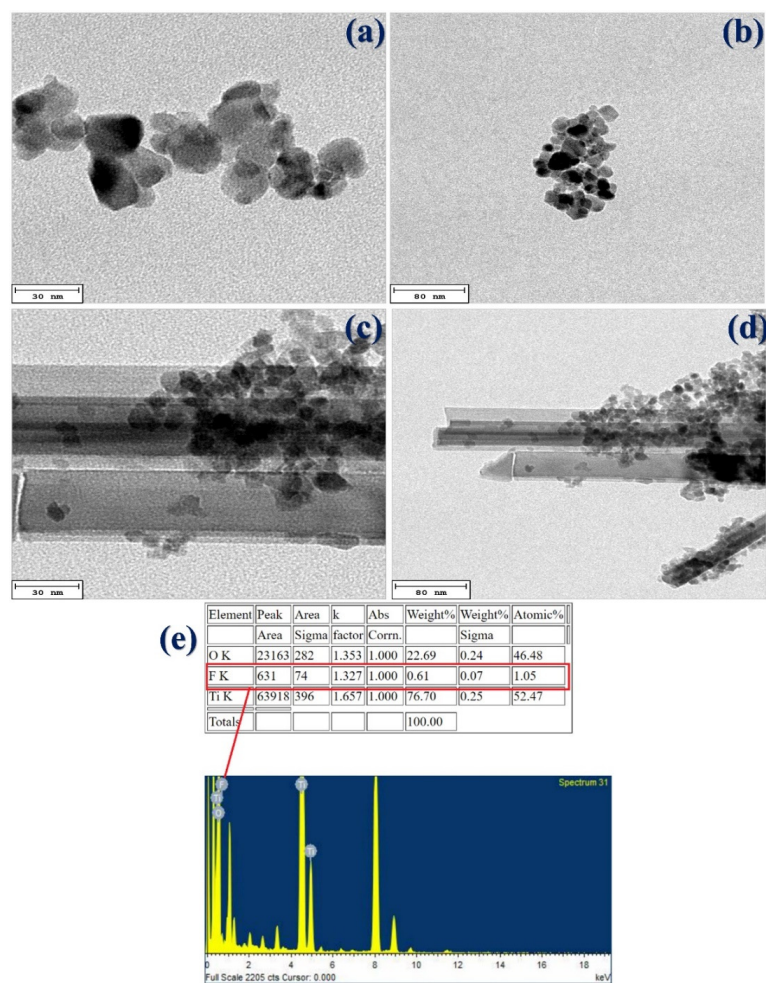


Figure 3. High resolution-transmission electron micrographs of bio-templated photocatalyst at 500 °C: (a) TiO₂ (30 nm), (b) TiO₂ (80 nm), (c) F-doped TiO₂ (30 nm), (d) F-doped TiO₂ (80 nm), and (e) High resolution-transmission electron micrographs energy dispersive X-ray spectrophotometer of F-doped TiO₂.

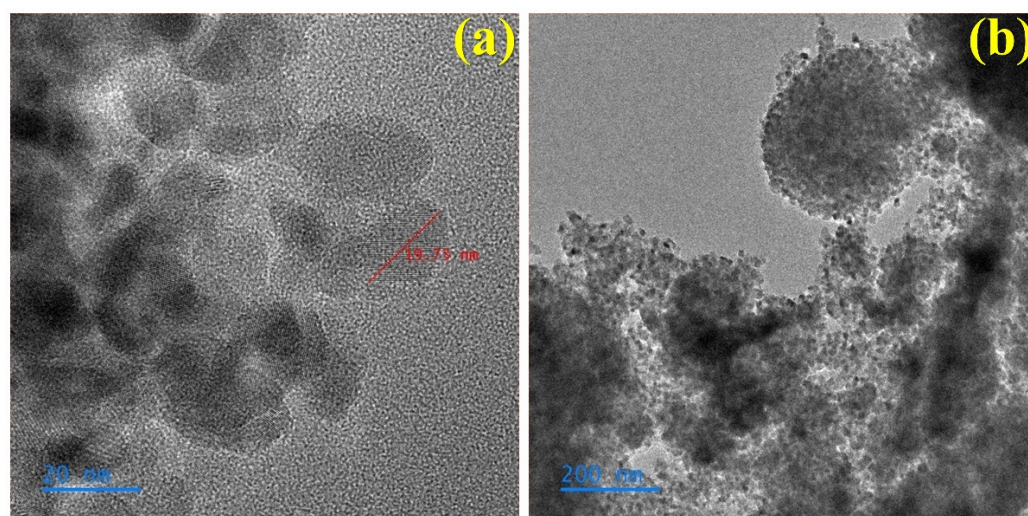


Figure 4. High resolution-transmission electron micrographs of bio-templated I-doped TiO₂ photocatalyst at 500 °C: (a) 20 nm, (b) 200 nm.

In this work, HR-TEM-EDXS confirmed the presence of F-doped TiO₂ composite material (Figure 3e). Analysis of the prepared F-doped TiO₂ confirmed the existence of F atoms. F accounts for about 1.05% in photocatalyst products. In the case of F-doped TiO₂ nanoparticles, an additional bamboo-like shape was exhibited in the HRTEM images, which could be responsible to reduce the size and increase the atomic percentage of synthesized materials. Therefore, it was confirmed that the elemental composition of the composite material F-doped TiO₂ contained F atom in addition to Ti and O elements.

3.3. Electronic Interaction of Synthesized Material

Using X-ray photoelectron spectroscopy (XPS), the surface composition and electronic interactions of synthetic materials, and relevant information about the bonding between two elements, can be obtained (Figure 5).

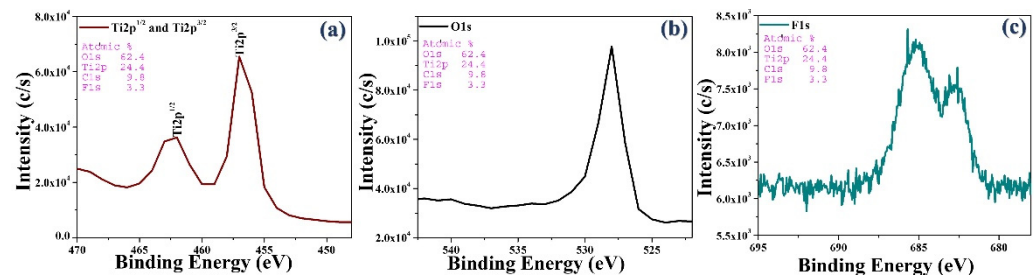


Figure 5. X-ray photoelectron spectra of bio-templated F-doped TiO₂ photocatalyst at 500 °C (a) Ti2p^{1/2} or 3/2, (b) O1s, and (c) F1s.

Using the best sample, the doping state of F and its light response wavelength were further analyzed. In order to understand and analyze the chemical state of the doped element F in the TiO₂ lattice, in energy spectrum peak testing of F-doped TiO₂, the sample with the highest photocatalytic degradation efficiency was employed. Figure 6 shows the XPS energy spectrum of F 1s of F-doped TiO₂ prepared at a calcination temperature of 500 °C. According to data provided by the National Bureau of Standards and Technology of the United States and the results of analysis of related documents [27–30], it can be inferred that in the figure below, the peak at 681.5 eV shows the formation of F replacing O in the TiO₂ lattice, the binding energy of the Ti-O-F chemical bond F 1s. In addition, the binding energy peak at about 685 eV is attributed to the F 1s binding energy of Ti-O-F formed when F interstitially enters the Ti-O lattice. This is consistent with the results reported in the literature [31,32].

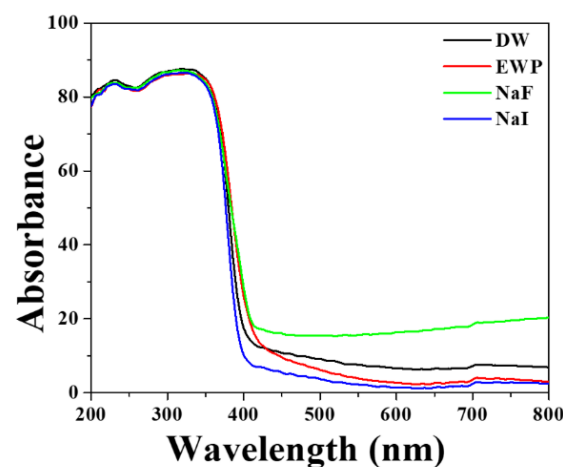


Figure 6. Ultraviolet-visible-near-infrared spectra of deionized water (DW), bio-templated TiO₂ photocatalyst (EWP), and bio-templated F/I-doped TiO₂ photocatalyst at 500 °C.

3.4. Energy Charge Transfer and Optical Properties of the F-Doped TiO₂ Synthesized Material

Figure 6 shows the UV-VIS-NIR absorption spectra of F/I-doped TiO₂ and undoped TiO₂ blanks prepared at a calcination temperature of 500 °C. It can be seen that the absorption edge of TiO₂ after F doping exhibits an obvious red-shift, and the light response wavelength is extended to the visible light region. The absorption edge and widening of the forbidden band of TiO₂ can be obtained by finding the wavelength and photon energy of the point corresponding to the maximum value of $|dA/d\lambda|$ [33] (where A is the absorption rate and λ is the wavelength). It was calculated that the absorption edge of the F-doped TiO₂ was red-shifted from 385 nm (before doping) to 428 nm. Obviously, the band gap was decreased from 3.2 eV (before doping) to 3.04 eV. The main reason for this should be that the 2p orbital energy of F doped in TiO₂ is close to the 2p orbital energy of O in TiO₂, which is prone to hybridization; this causes the valence band to shift upwards, resulting in a corresponding decrease in the band gap. Similar results were reported with the finding results of Wang et al. [34]. In addition, if the doped F introduces deep-level defects into the TiO₂ energy band, the acceptor energy level is close to the top of the valence band, and the donor energy level is close to the bottom of the conduction band, meaning that electrons can indirectly transition from the valence band to the conduction band. The energy of the absorbed photons is hence reduced.

3.5. Photocatalytic Degradation of Methylene Blue (MB)

Regarding evaluation of the activity of the photocatalysts, in addition to using UV-VIS-NIR to compare the characteristic absorptions, methylene blue (MB) was also employed in this study in photocatalytic experiments in order to further understand the photocatalytic effects of the various TiO₂ samples (Figure 7), where the observed color of doped sample was indicated in Figure 8.

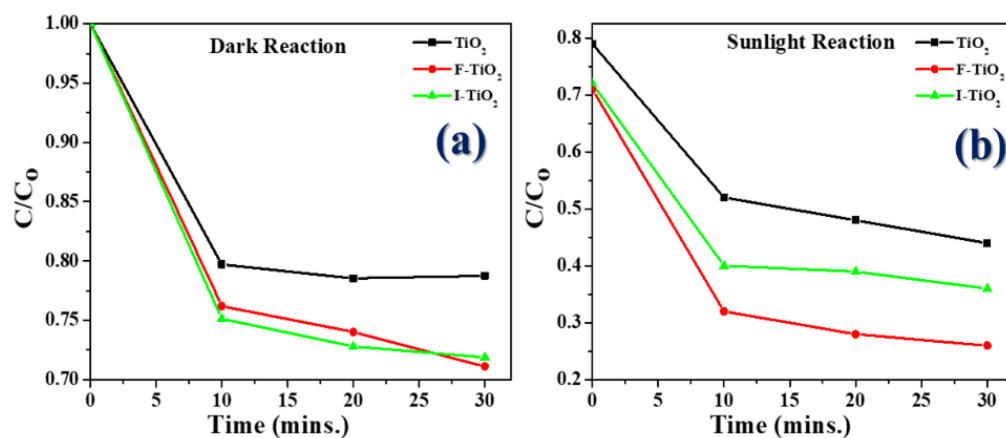


Figure 7. Photocatalytic degradation of MB using bio-templated TiO₂, F-doped TiO₂, and I-doped TiO₂ photocatalyst. (a) dark room, (b) sunlight.

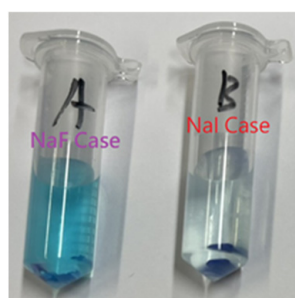


Figure 8. Dark blue solid residue was present at the bottom of the centrifuge tubes, (A) F-doped TiO₂, and (B) I-doped TiO₂ photocatalyst cases.

The F-doped TiO₂ photocatalytic material showed a high photocatalytic response not only under examination by UV-Vis, but also in the MB reaction test with a simulated sunlight source. These results agreed with those of another study, which showed F-doped TiO₂ particles synthesized by the sol-gel method to enhance the absorption of visible light [35].

- (a) In the first stage, the dark room test (Figure 7a), the catalyst particles of F-doped TiO₂ and I-doped TiO₂ (I-doped TiO₂ more strongly) absorbed the blue color of MB; the value of C/Co dropped from 1 to 0.75, and the bottom of the centrifuge tubes was obviously dark blue, which was speculated to represent physical adsorption. Please refer to the image included (Figure 8); as can be seen, a dark blue solid residue was present at the bottom of the centrifuge tubes. It was thought that the residual TiO₂ powder absorbed MB.
- (b) In the second stage with simulated sunlight, after the reaction in the dark room was completed, various TiO₂ samples were then irradiated with simulated sunlight. From the data shown in the figure (Figure 7b), it was apparent that the degradation rate of F-doped TiO₂ was the fastest of all the samples, at up to 73%, followed by I-doped TiO₂, and the degradation rate of TiO₂ was the lowest at 44%. As simulated sunlight also contains a small part of UV light, TiO₂ will also degrade in the MB aqueous solution test. The comparative removal percentage (%) of methylene blue dye has been shown in Table 1.

Table 1. The comparative study of doped TiO₂ nanoparticles.

Doped Nanoparticles	Contaminant Name	Light Source	Removal (%)	References
Pd-TiO ₂	Methylene blue and methyl orange	Visible light; 120 min	Methylene blue (99.4%) and methyl orange (92.6%)	[1]
V-TiO ₂	Methylene blue	Visible light; 300 min	15–30%	[2]
Carbon-doped TiO ₂	Methylene blue	Solar light	62.95%	[3]
Zirconium and silver co-doped TiO ₂	Methylene blue	Visible light	95%	[4]
F-doped TiO ₂	Methylene blue	Visible light	Discolored H ⁺ (41.5%) and OH (46.5%)	[5]
F-doped TiO ₂ prepared by expired egg white	Methylene blue	LED light	73%	This study

4. Reaction Mechanism

From the theory perspective of chemical MO (molecular orbital) and activation energy, the formation of O-F (single bond) could be easier than that of O=O (double bond), and the relative activation energy is lower. F-(fluorine atom with one electron) has an exceedingly stronger activity, and could be easily combined with O and become F-O bond (covalent molecular). In contrast, the binding energy of O=O is not easily breakable due to higher activation energy of O=O. Therefore, the O vacancy in the TiO₂ lattice is easily replaced by F, and its activation energy is relatively small.

On the other hand, the hidden meaning is that electrons are more easily excited in this case. Relatively, the band gap between the CB and VB is narrowed. Therefore, we speculate that the F-doped TiO₂ lattice can easily convert the photon energy (hν) to chemical energy in the visible-light range due to narrow band gap of F-doped TiO₂ produced in this study. However, the electrons can be easily excited on the surface of F-TiO₂ photocatalyst.

The doping of F into the molecular structure of TiO₂, and the activation energies of the related single or double bonds, are shown in Figure 9.

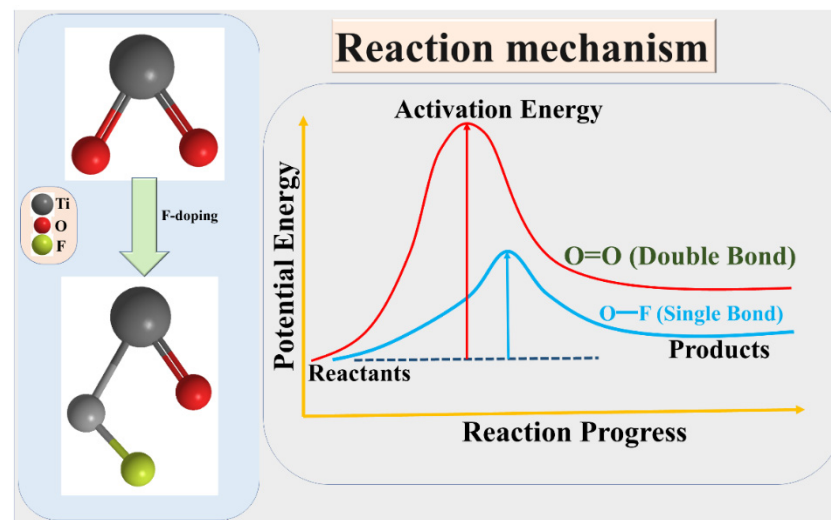


Figure 9. (Left) Doping of F into the molecular structure of TiO₂, and (Right) the activation energies of the related single or double bonds.

5. Conclusions

In current industrial applications, the main methods for synthesizing nanometer titanium dioxide powder are liquid-phase and gas-phase methods. Because traditional methods either are unable to be used to prepare nano-sized titanium dioxide, or the process is very difficult, a simpler process was designed in this study. Expired egg whites were employed as the template to prepare nano-TiO₂ photocatalysts by the sol-gel method; in addition, NaF/NaI were employed in certain proportions for doping of the TiO₂. The sol-gel method can be used to prepare single-component or multi-component molecular-level nano-catalysts of high purity, uniform particle size distribution, and high chemical activity at low temperature. Through UV/Vis and TEM, EDS, and XPS analyses, it was found that the prepared F-doped TiO₂ powder had an absorption reaction under visible light; the MB reaction test confirmed this result.

F-doped TiO₂ was prepared in this study. The F atom has one more electron than oxygen and replacing O₂[−] with F[−] in the lattice leaves an unpaired electron, as F can only accept one electron to obtain its closed shell structure. F-doped TiO₂ has catalytic activity under visible light; in this study UV/Vis, TEM, and XPS analyses proved that the photocatalytic activity of the prepared F-doped TiO₂ was better than that of P-25. However, the band gap was also observed as low as 3.04 eV. It is worthy of note that our process used expired eggs as the substrate, which is very in line with the issues of environmental protection and reuse. What is more, the F-doped TiO₂ catalyst prepared in this study will be able to replace the commercial P-25 material, which is a topic worthy of development and research.

According to TEM, the particles of F-doped TiO₂ were observed only 8.5 nm, which is smaller than the commercial P-25 particles; this means that the specific surface area of the F-doped TiO₂ catalyst prepared has been increased. In addition, in terms of composition, approximately 1% (atomic) F was found to be present via XPS. In case of MB reaction test, it was observed that our product had approximately more than two times photocatalytic degradation percentage than that of P-25.

Author Contributions: Conceptualization, C.-M.L. and W.-C.L.; methodology, C.-M.L. and C.-Y.C.; software, R.K.S.; formal analysis, R.K.S. and J.-S.C.; data curation, Y.-H.H. and P.-Y.L.; writing-original draft preparation, C.-M.L.; supervision, C.-Y.C. All authors have read and agreed to the published version of the manuscript.

Funding: The authors would like to thanks the Ministry of Science and Technology (Taiwan) for financial support (MOST 109-2811-M-194-502; MOST 108-2811-M-194-510).

Institutional Review Board Statement: Not applicable.

Informed Consent Statement: Not applicable.

Data Availability Statement: The data presented in this study are available on request from the corresponding author.

Conflicts of Interest: The authors declare no conflict of interest.

References

1. Bono, N.; Ponti, F.; Punta, C.; Candiani, G. Effect of UV irradiation and TiO₂-photocatalysis on airborne bacteria and viruses: An overview. *Materials* **2021**, *14*, 1075. [[CrossRef](#)] [[PubMed](#)]
2. Krakowiak, R.; Musial, J.; Bakun, P.; Spychała, M.; Czarczynska-Goslinska, B.; Mlynarczyk, D.T.; Koczorowski, T.; Sobotta, L.; Stanisz, B.; Goslinski, T. Titanium Dioxide-Based Photocatalysts for Degradation of Emerging Contaminants including Pharmaceutical Pollutants. *Appl. Sci.* **2021**, *11*, 8674. [[CrossRef](#)]
3. Jeon, J.P.; Kweon, D.H.; Jang, B.J.; Ju, M.J.; Baek, J.B. Enhancing the photocatalytic activity of TiO₂ catalysts. *Adv. Sustain. Syst.* **2020**, *4*, 2000197. [[CrossRef](#)]
4. Hoffmann, M.R.; Martin, S.T.; Choi, W.; Bahnemann, D.W. Environmental applications of semiconductor photocatalysis. *Chem. Rev.* **1995**, *95*, 69–96. [[CrossRef](#)]
5. Wang, R.; Billone, P.S.; Mullett, W.M. Nanomedicine in action: An overview of cancer nanomedicine on the market and in clinical trials. *J. Nanomater.* **2013**, *2013*, 1. [[CrossRef](#)]
6. Akpan, U.; Hameed, B. The advancements in sol–gel method of doped-TiO₂ photocatalysts. *Appl. Catal. A Gen.* **2010**, *375*, 1–11. [[CrossRef](#)]
7. Guo, Q.; Zhou, C.; Ma, Z.; Ren, Z.; Fan, H.; Yang, X. Elementary photocatalytic chemistry on TiO₂ surfaces. *Chem. Soc. Rev.* **2016**, *45*, 3701–3730. [[CrossRef](#)]
8. Asahi, R.; Morikawa, T.; Ohwaki, T.; Aoki, K.; Taga, Y. Visible-light photocatalysis in nitrogen-doped titanium oxides. *Science* **2001**, *293*, 269–271. [[CrossRef](#)]
9. Sakthivel, S.; Kisch, H. Daylight photocatalysis by carbon-modified titanium dioxide. *Angew. Chem. Int. Ed.* **2003**, *42*, 4908–4911. [[CrossRef](#)]
10. Miao, L.; Tanemura, S.; Watanabe, H.; Mori, Y.; Kaneko, K.; Toh, S. The improvement of optical reactivity for TiO₂ thin films by N₂–H₂ plasma surface-treatment. *J. Cryst. Growth* **2004**, *260*, 118–124. [[CrossRef](#)]
11. Luo, H.; Takata, T.; Lee, Y.; Zhao, J.; Domen, K.; Yan, Y. Photocatalytic activity enhancing for titanium dioxide by co-doping with bromine and chlorine. *Chem. Mater.* **2004**, *16*, 846–849. [[CrossRef](#)]
12. Kadam, A.N.; Salunkhe, T.T.; Kim, H.; Lee, S.-W. Biogenic synthesis of mesoporous N–S–C tri-doped TiO₂ photocatalyst via ultrasonic-assisted derivatization of biotemplate from expired egg white protein. *Appl. Surf. Sci.* **2020**, *518*, 146194. [[CrossRef](#)]
13. Niederberger, M.; Pinna, N. *Metal Oxide Nanoparticles in Organic Solvents: Synthesis, Formation, Assembly and Application*; Springer Science & Business Media: Berlin/Heidelberg, Germany, 2009.
14. Feinle, A.; Elsaesser, M.S.; Huesing, N. Sol–gel synthesis of monolithic materials with hierarchical porosity. *Chem. Soc. Rev.* **2016**, *45*, 3377–3399. [[CrossRef](#)] [[PubMed](#)]
15. Liao, Y.; Xu, Y.; Chan, Y. Semiconductor nanocrystals in sol–gel derived matrices. *Phys. Chem. Chem. Phys.* **2013**, *15*, 13694–13704. [[CrossRef](#)]
16. Haruta, M. Nanoparticulate Gold Catalysts for Low–Temperature CO Oxidation. *ChemInform* **2004**, *35*. [[CrossRef](#)]
17. Bayan, E.; Lupeiko, T.; Pustovaya, L.; Volkova, M. Synthesis and photocatalytic properties of Sn–TiO₂ nanomaterials. *J. Adv. Dielectr.* **2020**, *10*, 2060018. [[CrossRef](#)]
18. Purwaningsih, H.; Ervianto, Y.; Pratiwi, V.M.; Susanti, D.; Purniawan, A. Effect of cetyl trimethyl ammonium bromide as template of mesoporous silica mcm-41 from rice husk by sol-gel method. *IOP Conf. Ser. Mater. Sci. Eng.* **2019**, *515*, 012051. [[CrossRef](#)]
19. Wang, D.; Wu, X.; Gao, Q. Novel energy-saving window coating based on F doped TiO₂ nanocrystals with enhanced NIR shielding performance. *Ceram. Int.* **2021**, *47*, 28557–28565. [[CrossRef](#)]
20. Bindhu, M.; Willington, T.D.; Hatshan, M.R.; Chen, S.-M.; Chen, T.-W. Environmental photochemistry with Sn/F simultaneously doped TiO₂ nanoparticles: UV and visible light induced degradation of thiazine dye. *Environ. Res.* **2022**, *207*, 112108. [[CrossRef](#)]
21. Luis, A.; Neves, M.; Mendonça, M.; Monteiro, O. Influence of calcination parameters on the TiO₂ photocatalytic properties. *Mater. Chem. Phys.* **2011**, *125*, 20–25. [[CrossRef](#)]
22. Bayan, E.; Lupeiko, T.; Pustovaya, L.; Volkova, M.; Butova, V.; Guda, A. Zn–F co-doped TiO₂ nanomaterials: Synthesis, structure and photocatalytic activity. *J. Alloy. Compd.* **2020**, *822*, 153662. [[CrossRef](#)]
23. Sharma, R.K.; Wang, S.-C.; Maity, J.P.; Banerjee, P.; Dey, G.; Huang, Y.-H.; Bundschuh, J.; Hsiao, P.-G.; Chen, T.-H.; Chen, C.-Y. A novel BMSN (biologically synthesized mesoporous silica nanoparticles) material: Synthesis using a bacteria-mediated biosurfactant and characterization. *RSC Adv.* **2021**, *11*, 32906–32916. [[CrossRef](#)] [[PubMed](#)]
24. Maity, J.P.; Hsu, C.-M.; Lin, T.-J.; Lee, W.-C.; Bhattacharya, P.; Bundschuh, J.; Chen, C.-Y. Removal of fluoride from water through bacterial-surfactin mediated novel hydroxyapatite nanoparticle and its efficiency assessment: Adsorption isotherm, adsorption kinetic and adsorption thermodynamics. *Environ. Nanotechnol. Monit. Manag.* **2018**, *9*, 18–28. [[CrossRef](#)]

25. Xia, S.-M.; Zhang, Y.-Q.; Zheng, Y.-F.; Xu, C.-S.; Liu, G.-M. Enhanced visible light photocatalytic activity of N, F-codoped TiO₂ powders with high thermal stability. *Environ. Technol.* **2019**, *40*, 1418–1424. [[CrossRef](#)]
26. Gao, Q.; Si, F.; Zhang, S.; Fang, Y.; Chen, X.; Yang, S. Hydrogenated F-doped TiO₂ for photocatalytic hydrogen evolution and pollutant degradation. *Int. J. Hydrog. Energy* **2019**, *44*, 8011–8019. [[CrossRef](#)]
27. Burda, C.; Lou, Y.; Chen, X.; Samia, A.C.; Stout, J.; Gole, J.L. Enhanced nitrogen doping in TiO₂ nanoparticles. *Nano Lett.* **2003**, *3*, 1049–1051. [[CrossRef](#)]
28. Ihara, T.; Miyoshi, M.; Iriyama, Y.; Matsumoto, O.; Sugihara, S. Visible-light-active titanium oxide photocatalyst realized by an oxygen-deficient structure and by nitrogen doping. *Appl. Catal. B: Environ.* **2003**, *42*, 403–409. [[CrossRef](#)]
29. Kosowska, B.; Mozia, S.; Morawski, A.W.; Grzmil, B.; Janus, M.; Kałucki, K. The preparation of TiO₂–nitrogen doped by calcination of TiO₂·xH₂O under ammonia atmosphere for visible light photocatalysis. *Sol. Energy Mater. Sol. Cells* **2005**, *88*, 269–280. [[CrossRef](#)]
30. Yin, S.; Ihara, K.; Komatsu, M.; Zhang, Q.; Saito, F.; Kyotani, T.; Sato, T. Low temperature synthesis of TiO₂–xNy powders and films with visible light responsive photocatalytic activity. *Solid State Commun.* **2006**, *137*, 132–137. [[CrossRef](#)]
31. Wang, Q.; Chen, C.; Zhao, D.; Ma, W.; Zhao, J. Change of adsorption modes of dyes on fluorinated TiO₂ and its effect on photocatalytic degradation of dyes under visible irradiation. *Langmuir* **2008**, *24*, 7338–7345. [[CrossRef](#)]
32. Song, H.; Xu, L.; Chen, M.; Cui, Y.; Wu, C.-E.; Qiu, J.; Xu, L.; Cheng, G.; Hu, X. Recent progresses in the synthesis of MnO₂ nanowire and its application in environmental catalysis. *RSC Adv.* **2021**, *11*, 35494–35513. [[CrossRef](#)] [[PubMed](#)]
33. Michalow, K.A.; Logvinovich, D.; Weidenkaff, A.; Amberg, M.; Fortunato, G.; Heel, A.; Graule, T.; Rekas, M. Synthesis, characterization and electronic structure of nitrogen-doped TiO₂ nanopowder. *Catal. Today* **2009**, *144*, 7–12. [[CrossRef](#)]
34. Wang, Q.; Rhimi, B.; Wang, H.; Wang, C. Efficient photocatalytic degradation of gaseous toluene over F-doped TiO₂/exfoliated bentonite. *Appl. Surf. Sci.* **2020**, *530*, 147286. [[CrossRef](#)]
35. Liu, D.; Tian, R.; Wang, J.; Nie, E.; Piao, X.; Li, X.; Sun, Z. Photoelectrocatalytic degradation of methylene blue using F doped TiO₂ photoelectrode under visible light irradiation. *Chemosphere* **2017**, *185*, 574–581. [[CrossRef](#)]